

Correlating head kinematics and cervical cerebrospinal fluid pressure transients in simulated whiplash exposures

Downloaded from: https://research.chalmers.se, 2025-10-19 05:12 UTC

Citation for the original published paper (version of record):

Soltan, N., Svensson, M., Jones, C. et al (2025). Correlating head kinematics and cervical cerebrospinal fluid pressure transients in simulated whiplash exposures. Journal of Biomechanics, 193. http://dx.doi.org/10.1016/j.jbiomech.2025.112994

N.B. When citing this work, cite the original published paper.

research.chalmers.se offers the possibility of retrieving research publications produced at Chalmers University of Technology. It covers all kind of research output: articles, dissertations, conference papers, reports etc. since 2004. research.chalmers.se is administrated and maintained by Chalmers Library

ELSEVIER

Contents lists available at ScienceDirect

Journal of Biomechanics

journal homepage: www.elsevier.com/locate/jbiomech



Correlating head kinematics and cervical cerebrospinal fluid pressure transients in simulated whiplash exposures

Nikoo Soltan ^{a,b}, Mats Y. Svensson ^c, Claire F. Jones ^d, Peter A. Cripton ^{b,e}, Gunter P. Siegmund ^{f,g,*} ©

- ^a Department of Mechanical Engineering, The University of British Columbia, Vancouver, BC, Canada
- ^b Orthopaedic and Injury Biomechanics Group, ICORD, Blusson Spinal Cord Centre, 818 West 10th Avenue, Vancouver, BC V5Z1M9, Canada
- ^c Division of Vehicle Safety, Mechanics and Maritime Sciences, Chalmers University of Technology, Gothenburg SE-412 96, Sweden
- d School of Electrical and Mechanical Engineering, The University of Adelaide, Level 7, Adelaide Health and Medical Sciences Building, North Terrace, Adelaide, SA 5000, Australia
- ^e School of Biomedical Engineering, The University of British Columbia, Vancouver, BC, Canada
- ^f School of Kinesiology, The University of British Columbia, Vancouver, BC, Canada
- g MEA Forensic Engineers & Scientists, 23281 Vista Grande Drive, Laguna Hills, CA 92653, United States

ARTICLE INFO

Keywords: Whiplash injury Cervical spine Cerebrospinal fluid pressure Pig model

ABSTRACT

The origin and mechanics of whiplash injury from motor vehicle collisions are poorly understood. Among the proposed injury mechanisms, the inertial loading of the head and neck during whiplash exposures is theorized to produce injurious cerebrospinal fluid pressure (CSFP) transients. To better understand the mechanics and modal behavior of CSFP transients during whiplash exposures, we quantified the time–frequency relationship between input head kinematics and cervical CSFP responses in an *in vivo* pig model. Wavelet coherence analysis was used to correlate seven head kinematic parameters (including temporal Neck Injury Criterion, NIC) with CSFP during simulated extension and flexion whiplash exposures. Overall, the first and last 50 ms of exposures, and frequency ranges between 30–65 Hz had larger coherences between head kinematics and CSFP, with higher coherences in extension exposures than flexion exposures. NIC did not universally outperform other head kinematic parameters as a correlate of CSFP. These findings highlight the complexity of the dynamics involved in generating CSFP transients in the cervical spine during whiplash exposures.

1. Introduction

Whiplash injuries from motor vehicle collisions can cause symptoms including neck pain, headache, and sensory deficits (Elliott et al., 2009; Sterling et al., 2004). Symptoms experienced by whiplash patients are thought to be related to the transmitted forces and resulting strains in the tissues of the neck (Siegmund et al., 2009). However, the organic sources of some whiplash symptoms remain poorly understood, in part because morphological signs of tissue damage can be subtle and challenging to detect clinically (Elliott et al., 2009).

Several anatomical sites of whiplash injury have been proposed including the facet joints, spinal ligaments, intervertebral discs, vertebral arteries, neck muscles, and neural tissues (Curatolo et al., 2011; Siegmund et al., 2009). Recent evidence of altered spinal cord white matter integrity (Hoggarth et al., 2020) and neuroinflammation of

cervical dorsal root ganglia (Ridehalgh et al., 2025), coupled with central sensitization (Elliott et al., 2009; Van Oosterwijck et al., 2013) and neuropathic pain (Fundaun et al., 2022) symptoms in some whiplash patients, points to the potential involvement of neural tissues. Along with possible impingement of nerve roots from intervertebral foraminal narrowing in some cases (Panjabi et al., 2006), one relatively understudied theory postulates that collision-induced head and neck motions can cause injurious cerebrospinal fluid pressure (CSFP) transients in the cervical spine (Aldman, 1986). These CSFP transients have the potential to hydrodynamically stress and strain neural tissues, including the spinal cord, nerve roots, and dorsal root ganglia.

Prior pre-clinical animal studies have characterized the unphysiological CSFP transients in the cervical spine during whiplash exposures (Soltan et al., 2025; Svensson et al., 1993) and the associated nerve cell damage in the dorsal root ganglia (Örtengren et al., 1996). Although

E-mail addresses: gunter.siegmund@ubc.ca, gunter.siegmund@meaforensic.com (G.P. Siegmund).

^{*} Corresponding author.

these prior studies support the plausibility of this injury mechanism, there is limited mechanistic understanding of how head and neck dynamics contribute to, and what anatomical components are involved in, the observed CSFP transients. A better understanding could help optimize whiplash injury criteria and inform the design of occupant protection systems.

The Neck Injury Criterion (NIC, Eq. (1)) is one existing injury criterion related to CSFP transients (Bostrom et al., 1996).

$$NIC = 0.2 \bullet a_{rel} + v_{rel}^2 \tag{1}$$

where a_{rel} and v_{rel} are the relative horizontal acceleration and velocity, respectively, between the torso and head. A neck scaling factor (0.2) is applied to a_{rel} (Bostrom et al., 1996).

NIC was developed analytically from a rudimentary fluid flow model on the basis that larger relative motion between the upper and lower cervical spine in the anterior-posterior direction (in humans) poses a greater risk of whiplash injury. For a rear-end collision, NIC is calculated using the relative horizontal acceleration and velocity between the torso and head, and the peak value immediately before head restraint contact is used to quantify whiplash injury risk. NIC is a simplification of the complex head and neck dynamics during a collision event. To further our understanding of these events, the effect of all collision-induced linear and rotational head and neck kinematics on cervical CSFP responses need to be empirically assessed over the entire time-course of the exposure.

Wavelet coherence analysis is a method of assessing the localized linear correlation between two time-series signals (Grinsted et al., 2004; Maraun and Kurths, 2004). This method can provide greater insights about the relationship between two signals than more reductive techniques such as correlating peak values extracted from temporal data. As an expansion of Fourier-based techniques, wavelet-based methods do not rely on the assumption of stationarity in the time-series data, can more effectively capture transients and non-periodic characteristics, and can decompose signals in the time-frequency domains (Grinsted et al., 2004).

Thus, to better understand the mechanics and modal behavior of CSFP transients in the neck during whiplash exposures, our goal was to quantify the time–frequency relationship between input head kinematics and cervical CSFP in an *in vivo* porcine model of whiplash injury. Using wavelet coherence analysis, our specific aims were to: (i) identify the time spans and frequencies with maximal coherence between head kinematics and CSFP; and (ii) determine which head kinematic parameters correlate best with CSFP.

2. Methods

This study was approved by the University of British Columbia Animal Care Committee (A19-0290) and complied with the guidelines of the Canadian Council on Animal Care. A detailed description of experimental procedures can be found elsewhere (Soltan et al., 2025) but pertinent information is outlined here.

2.1. Animals

Four female Yorkshire pigs (P1-P4, 22.6 \pm 2.6 kg) were anesthetized, intubated, and mechanically ventilated during testing. At the end of procedures, without anesthetic recovery, animals were humanely euthanized with intravenous sodium pentobarbital.

2.2. Cerebrospinal fluid pressure

CSFP was measured along the cervical spine using three fiber-optic pressure transducers (FOP-LS-2FR-20, FISO, Quebec, Canada). To avoid disrupting the soft and hard tissues of the neck, a laminectomy was performed in the lower thoracic spine (T11 or T12) for placement of

a custom intrathecal catheter, and the pressure transducers were advanced to the C2, C5, and C7 vertebral levels via the catheter. The catheter-dura interface was sealed using cyanoacrylate adhesive (Loctite 495, Dusseldorf, Germany). For one subject (P4), the pressure transducer intended for C7 could only be advanced to T6.

Though pain patterns in whiplash patients can span the entire neck (Aprill et al., 1990), CSFP at the C5 level was used for subsequent analyses in this study (referred to as CSFP hereafter) since the dermatomes of the lower cervical spine are more commonly implicated in whiplash symptoms (Chien et al., 2010, 2009, 2008), and data at this level were more complete than at C7. Additionally, the CSFP responses at all three levels typically had comparable waveforms in each test (Soltan et al., 2025).

2.3. Head kinematics

Sagittal head kinematics were measured using a head-mounted sensor array (Fig. 1A) consisting of an angular rate sensor (ARS Pro-1500, Diversified Technical Systems, Seal Beach, CA, USA) and orthogonal linear accelerometers (7265A, Endevco, Irvine, CA, USA). The sensor array and four head landmarks were digitized (FaroArm B08-02, Lake Mary, FL, USA) to facilitate transforming kinematics to the atlanto-occipital joint (AOJ) in a standardized pig head anatomical coordinate system (Fig. 1B), as described elsewhere (Soltan et al., 2023).

2.4. Whiplash exposures

Whiplash exposures were simulated using a custom apparatus consisting of two servomotors, several mechanical linkages, and an affixed biteplate (Fig. 1A and C). Through the combined rotation of both motors, the biteplate and head were actuated to produce head trajectories that simulated rear-end or frontal whiplash exposures. The programmed motion profiles were provided to the servomotor system controller in 10 ms intervals (100 Hz). During the exposures, the animal's torso was constrained to a table using a harness and ratchet straps distributed along the torso up to the base of the neck (approximate level of T1).

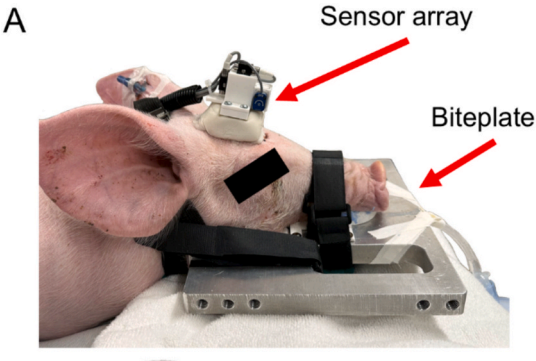
Simulated whiplash exposures consisted of two head trajectories (E1 and E2) representing rear-end collisions, and two head trajectories (F1 and F2) representing frontal collisions (Fig. 2A and B). The E1 and E2 head trajectories involved combined retraction and extension of the head, with the former having a more pronounced retraction component representing the inertia-driven head lag seen in human subject tests (Siegmund et al., 1997; Svensson et al., 2000). Similarly, the F1 and F2 head trajectories involved combined protraction and flexion of the head, with the former having a more pronounced protraction component (Svensson et al., 2000). The animals and number of tests per head trajectory are given in Table 1.

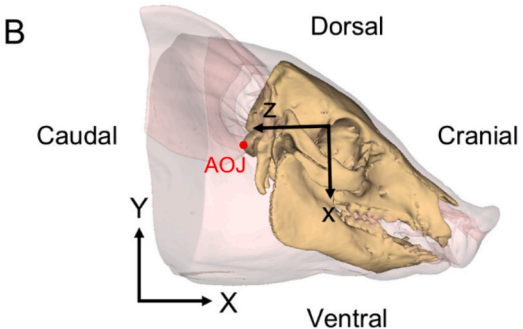
The temporal angular displacement traces of the four head trajectories were comparable to previous human volunteer (Deng et al., 1998) and *ex vivo* human (full body, (Bertholon et al., 2000); head-neck segments, (Kang et al., 2018)) sled tests with speed changes of between 3–4 m/s with no head restraint, and to previous *in vivo* porcine tests (Svensson et al., 1993) (Fig. 2C). The head trajectories tested in this study generated robust variations in CSFP (Fig. 2D). Additionally, the severity of these trajectories were translationally relevant since peak NIC values (as calculated in Section 2.5) were above the proposed NIC injury threshold (Bostrom et al., 1996) (Table 2).

2.5. Data acquisition and processing

Kinematics data were hardware filtered according to SAE J211 Channel Class 1000 (SAE, 2003) and CSFP data were conditioned using signal conditioner units (FPI-LS-10, FISO, Quebec, Canada). All data were acquired at 10 kHz (PXI-6221, National Instruments, Austin, USA) and analyzed using MATLAB (R2021b, Mathworks, Natick, USA).

With motion onset defined as t = 0 ms, signals were cropped from t = 0





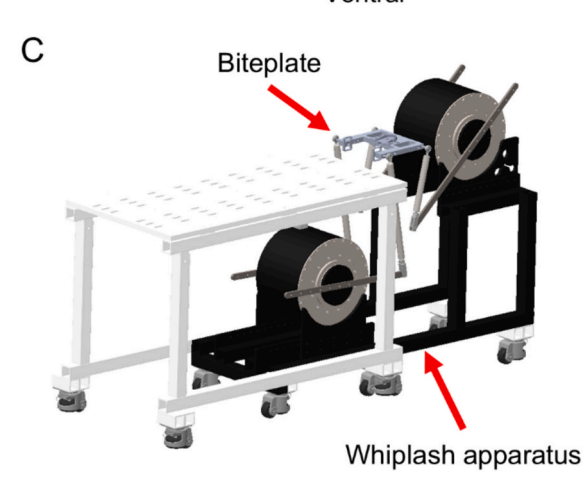


Fig. 1. (A) Sensor array and biteplate secured to the anesthetized animal's head. The sensor array was mounted using wood screws and a polymethyl methacrylate (PMMA) mantle. The biteplate consisted of 3D printed mouthguards attached to an aluminum base. The PMMA-filled mouthguards were coupled to the animal's upper and lower dentition and to wood screws inserted into the upper palate and mandible. The biteplate was further secured to the head using straps around the snout and head. (B) Sagittal pig head anatomical coordinate system (z-x), global reference frame (X-Y), and the location of the atlanto-occipital joint (AOJ). (C) Model of the whiplash apparatus, biteplate, and test table. The servomotors (SGMCS-2ZN, Yaskawa, Japan) were powered by servo drives (not shown, SGDV Servopack, Yaskawa, Japan) and controlled using a motion controller (not shown, NI 7350 and PXI-8108, National Instruments, Austin, USA).

-50~ms to 100 ms after the end of each programmed motion profile (tfinal = 260 (E1), 230 (E2), 253 (F1), 253 (F2) ms). The cropped signals were digitally low-pass filtered at 100 Hz using a dual-pass 4th-order Butterworth filter. Head angular acceleration (α) was calculated by numerical differentiation of the filtered angular rate (ω) signal. Sagittal head linear accelerations (a_x,a_z) were transformed from the sensor array to a generic pig AOJ in the head coordinate system (Soltan et al., 2023) (Fig. 1B) using rigid body assumptions. Sagittal AOJ linear velocities (v_x,v_z) were calculated by numerical integration (cumtrapz function in MATLAB) of the transformed acceleration data. Temporal NIC was

calculated using Eq. (2) (Bostrom et al., 1996), where $a_{\rm rel,Y}$ and $v_{\rm rel,Y}$ are the vertical acceleration and velocity, respectively, of the AOJ relative to the T1 vertebra in the global reference frame. T1 was assumed to be stationary (approximated by constraining the thorax up to the base of the neck to the test table). Vertical kinematics used here (with animal lying prone or supine) are anatomically analogous to the horizontal kinematics of a seated human occupant used in the NIC equation when applied to humans. A neck length scaling factor of 0.2 was assumed for consistency with prior whiplash studies where pigs of similar size to this study were used (Bostrom et al., 1996).

$$NIC(t) = 0.2 \bullet a_{rel,Y}(t) + \left(\nu_{rel,Y}(t)\right)^{2} \tag{2}$$

To account for inter-animal variability and physiological variation in baseline CSFP, mean CSFP over 1-second before motion onset in each test was subtracted from the CSFP signal.

2.6. Wavelet coherence analysis

A MATLAB package (Grinsted et al., 2004) was used to determine the wavelet coherence (Fig. 3A) between CSFP and each of seven kinematic parameters (k: NIC, α , ω , a_x , v_x , a_z , v_z) for each test. The Morlet mother wavelet (center frequency: 6 rad, scale resolution: 15 scales/octave) was used since it is well localized in both time and frequency, and can effectively capture transient events (Grinsted et al., 2004). For each whiplash exposure, a 3D plot was produced depicting time (x-axis), frequency (y-axis) and wavelet coherence (color scale) for each of the seven CSFP/kinematic-parameter pairs (Fig. 3B). Statistically significant coherence regions (alpha = 0.05, generally yellowish regions outlined by black contour lines in Fig. 3B) were determined using Monte Carlo methods. These regions were determined by comparing the coherence at each time and frequency against a statistical distribution generated by surrogate data pairs (n = 1000) modelling a stochastic Gaussian process (Grinsted et al., 2004). The 3D plots also indicate a cone of influence region (lighter shaded area under white line) where the results may be distorted by edge effects at the beginning and end of the dataset. Only the areas outside the cone of influence (i.e., areas unaffected by edge effects) were further considered. Additionally, a time range from servomotor motion onset (t = 0) to maximum head angular displacement (e.g., t = 144.7 ms in Fig. 3) and a frequency range from 10 to 100 Hz were considered in subsequent extraction of wavelet metrics (Section 2.7). The upper time limit eliminated sharp peaks present in all kinematic and pressure signals associated with abrupt halting of head motion (Fig. 2C), which could skew the coherence measures. The frequency range was dictated by the length of the input data (on the order of 100 ms corresponding to 10 Hz) and the frequency of the servomotor motion control (100 Hz), respectively.

2.7. Wavelet-derived metrics and statistical analysis

Using the CSFP-kinematic parameter coherence plots for each kinematic parameter (k = 1 to 7) in each whiplash test (i = 1 to between 6 and 14 depending on the type of whiplash exposure), the proportion of significant coherence (p) at every time increment (t) and frequency band (f) was determined ($p_{ki}(t)$ and $p_{ki}(f)$, respectively). These proportions were determined outside the cone of influence, and within time from motion onset to maximum angular displacement, and frequency from 10 to 100 Hz.

To determine the time intervals with maximal coherence between CSFP and head kinematics, across-test means of $p_{ki}(t)$ were calculated for each kinematic parameter ($\bar{p}_k(t)$) and plotted over time for each whiplash exposure (E1, E2, F1, F2) separately.

To determine the frequencies with maximal coherence between CSFP and head kinematics, across-test means of $p_{ki}(f)$ were determined for each kinematic parameter $(\bar{p}_k(f))$ and plotted against frequency for each whiplash exposure (E1, E2, F1, F2) separately. An aggregated average

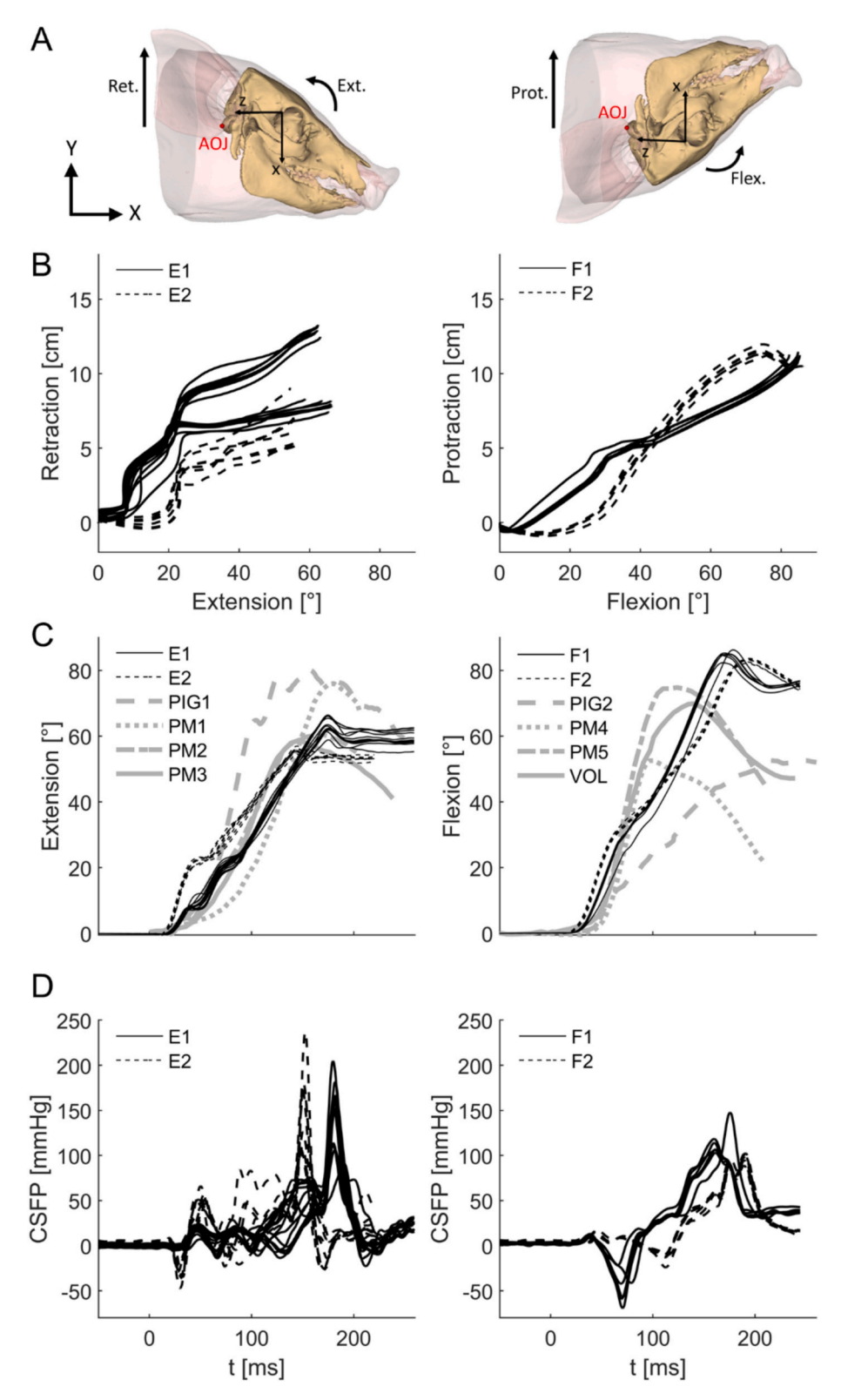


Fig. 2. (A) Extension (ext.)/retraction (ret.) and flexion (flex.)/protraction (prot.) exposures were imposed with the animal positioned prone (left) and supine (right) on the test table, respectively. Retraction (ret.) and protraction (prot.) are the vertical displacement of the atlanto-occipital joint (AOJ) in the global reference frame (Y direction). Extension (ext.) and flexion (flex.) are the angular displacements of the head. Each exposure was initiated from a programmed initial position where the biteplate was vertically aligned with the stationary torso. (B) Retraction vs. extension (from t = 0 up to point of maximum extension), and protraction vs flexion (from t = 0 up to point of maximum flexion) for the extension (left) and flexion (right) tests, respectively. Linear and angular displacement data calculated from head-mounted sensors (see Section 2.5). (C) Head angular displacement over time for the extension (left) and flexion (right) tests in this study and tests from literature (extension: *in vivo* porcine, PIG1 (Svensson et al., 1993); *ex vivo* human, PM1 to PM3 (Bertholon et al., 2000); flexion: *in vivo* porcine, PIG2 (Svensson et al., 1993); *ex vivo* human head-neck, PM4 and PM5 (Kang et al., 2018); human volunteer, VOL (Deng et al., 1998). (D) CSFP responses for the E1/E2 (left) and F1/F2 (right) tests.

Table 1

Animal number, body mass, and number of repeated tests for each whiplash exposure. The whiplash exposure tests reported herein (8 or 9 tests/animal) were interspersed among a larger test series (27 tests/animal) in which the severity of exposures was incrementally increased. The animal was momentarily disconnected from the ventilator during each test and subsequently reconnected for a 3–5-minute recovery period between each test. Animals that received both extension and flexion exposures received the extension exposures first.

Animal	Body Mass [kg]	# of Tests			
		E1	E2	F1	F2
P1	23.1	7	1	_	_
P2	21.8	7	1	_	_
P3	24.6	_	3	6	-
P4	21.0	_	3	_	6
	Total	14	8	6	6

Table 2 Mean and standard deviation (SD) for peak NIC, time to peak NIC, peak angular rate (ω) and peak angular displacement (θ) for each head trajectory. The mean peak NIC values were all above the injury threshold of 15 m²/s² (Bostrom et al., 1996).

	E1	E2	F1	F2
Peak NIC [m ² /s ²]	34.1 (7.9)	29.2 (4.6)	22.2 (3.8)	18.7 (0.9)
Time to Peak NIC [ms]	37.5 (1.8)	31.5 (1.4)	38.1 (1.9)	43.4 (3.3)
Peak ω [rad/s]	11.6 (0.7)	19.9 (1.3)	14.6 (0.3)	17.3 (0.8)
Peak θ [deg]	63.5 (2.3)	55.8 (0.7)	84.5 (1.3)	83.0 (0.5)

across all kinematic parameters $(\overline{\overline{p}}(f))$ was also calculated and plotted for each of the four whiplash exposures. At maximum $\overline{\overline{p}}(f)$, frequency (F) and the full width at half-maximum range of frequencies (F_{FWHM}) were then determined for each of the four types of whiplash exposures. The F_{FWHM} represents the frequency range that captures the majority of the significant coherence regions.

To assess each kinematic parameter as a correlate of CSFP response, the $p_{ki}(f)$ bounded by the F_{FWHM} was calculated for each pressure-kinematic pair $(p_{ki}(F_{FWHM}))$. Mean $(\bar{p}_k(F_{FWHM}))$ and standard deviation for the CSFP-kinematic parameter pairs are reported for each whiplash exposure. A repeated-measures analysis of variance (ANOVA; independent: kinematic parameter, k; dependent: $p_{ki}(F_{FWHM})$) was conducted using SPSS statistics (v29, IBM, Illinois, USA). If a significant Greenhouse-Geisser corrected F-statistic was found, post-hoc pairwise comparisons were made and Bonferroni adjusted p-values are reported for multiple comparisons.

3. Results

The time-varying proportion of significant coherence between CSFP and head kinematics exhibited a relatively consistent bimodal pattern within and across the four whiplash exposures (Fig. 4). Peak coherences occurred at the start and end of the motion pulse with a local minimum near the middle of the pulse. The proportion of significant coherence values reached 80 to 90 % for the extension exposures, but only 40 to 50 % for the flexion exposures (Fig. 4).

Similarly, the frequency-varying proportion of significant coherence between CSFP and head kinematics were larger for the extension exposures than for the flexion exposures (Fig. 5). For the extension exposures, peak aggregate coherence was 67.6 % at 38.9 Hz for E1, and 74.9 % at 30.9 Hz for E2 (Table 3). For the flexion exposures, peak aggregate coherence was lower and occurred at a higher frequency, reaching 30.5 % at 61.8 Hz for F1, and 39.4 % at 64.7 Hz for F2 (Table 3). Both flexion exposures also had a smaller peak in aggregate coherence near 20 Hz (Fig. 5). The E1 exposure had the smallest $F_{\rm FWHM}$ range (27 Hz), while the F1 exposure had the largest $F_{\rm FWHM}$ range (> 53.2 Hz).

Except for the E1 whiplash exposure, the different kinematic

parameters generally did not differ from one another as correlates of CSFP (Fig. 6). For the E1 whiplash exposure, the best correlates of CSFP were α , ω , a_x , and v_x , all of which were significantly better correlated than NIC (p-value < 0.05). For the other three whiplash exposures, NIC was better correlated to CSFP than only one kinematic parameter (α in F2). Tabulated pairwise comparisons can be found in Supplementary Tables S1–S4.

4. Discussion

Pressure transients in the cervical CSF could be a potential mechanism of whiplash injury (Soltan et al., 2025; Svensson et al., 1993), but the mechanics that lead to these pressure transients are poorly understood. We used a pig model of whiplash injury to characterize the time–frequency relationship between head kinematics and CSFP. Overall, the relationships between head/neck kinematics and CSFP varied over time and across frequencies, with stronger relationships between most head kinematic parameters and CSFP during the extension exposures and weaker relationships between fewer kinematic parameters and CSFP during the flexion exposures.

Across the four whiplash exposures tested, time-varying coherences between head kinematics and CSFP were maximal in the first and last 50 ms of the exposure. These intervals of high coherence indicate potentially critical intervals for CSFP transient responses. The conventional use of NIC involves extracting the peak value immediately before or at head restraint contact which was found to occur approximately 60 ms after C7-T1 joint motion onset (approximating t=0 in our study) in 2 m/s rear-end sled tests (Siegmund et al., 1997). This suggests that peak NIC extracted before head restraint contact may suitably fall within this high coherence region. Peak NIC in our tests occurred between 30–40 ms (Table 2).

Peak aggregate coherences between head kinematics and CSFP occurred at 30.9 and 38.9 Hz for the extension tests, and 61.8 and 64.7 Hz for the flexion tests. These frequencies are considerably higher than the reported natural frequencies of the human head-neck system. During thoracic vibration loading of human volunteers, the natural frequencies of the head-neck system were 1.68 \pm 0.69 Hz (relaxed muscles) and 1.96 \pm 0.66 Hz (tensed muscles) in the first flexion-extension vibration mode, and 7.91 \pm 0.74 Hz, (relaxed) and 9.78 \pm 0.67 Hz (tensed) in the second head retraction-protraction vibration mode (Bourdet et al., 2005). This comparison suggests that the modal behavior of the cervical CSFP response to head kinematics differs from gross head-neck displacement. The peak coherences at the higher frequencies could potentially be related to intervertebral motion (Aldman, 1986; Holmes et al., 1996; Svensson et al., 1993). From an engineering perspective, the natural frequencies of intervertebral segments are expected to be larger than the natural frequency of the entire head-neck system due to the greater intersegmental stiffness (Moroney et al., 1988) and smaller vertebral mass.

Across the kinematic parameters considered in this study, head kinematics were better correlated to CSFP in extension exposures (max $\overline{\overline{p}}(f) \ge 67.6$ %) than flexion exposures (max $\overline{\overline{p}}(f) \le 39.4$ %). The smaller proportion of significant coherence in the flexion exposures may indicate differences in the cascade of head-to-cervical spine intervertebral motion and spinal canal volume changes between the exposure orientations. Previous studies have demonstrated that the intersegmental stiffnesses and ranges of motion of the human (Panjabi et al., 2001; Shea et al., 1991) and pig (Wilke et al., 2011) cervical spine differ in extension and flexion loading. In the pig, range of motion was generally larger in flexion than in extension in the cervical segments caudal to C2 (largest mean difference: 4.9° at C5-C6) (Wilke et al., 2011). This larger cervical vertebral range of motion could contribute to a greater decoupling of head kinematics and cervical CSFP in flexion exposures. Further work is needed to characterize the differences in intervertebral motion in dynamic extension and flexion whiplash exposures in the pig and the effect

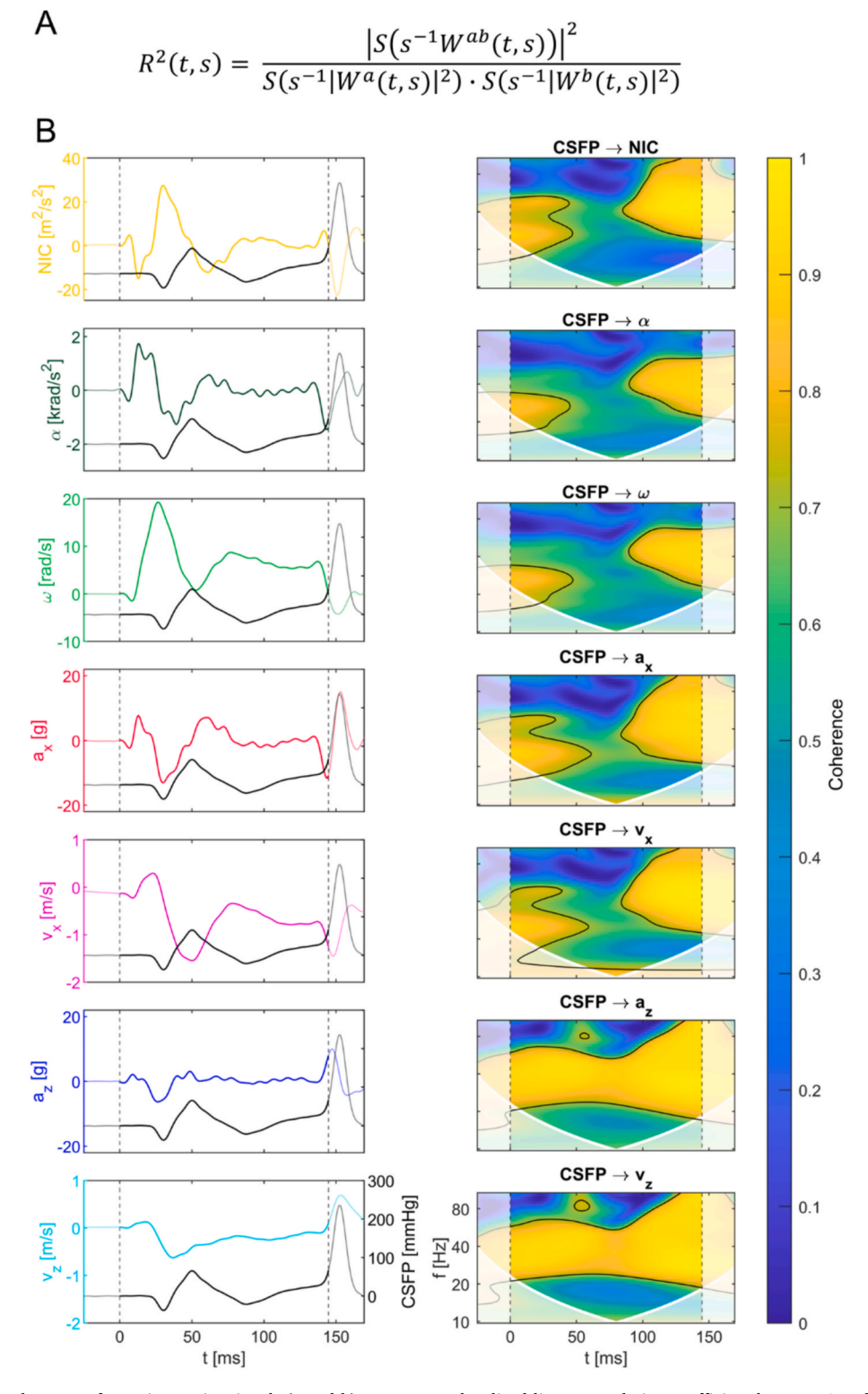


Fig. 3. (A) The wavelet coherence of two time-series signals (a and b) represents a localized linear correlation coefficient between 0 and 1 in the time-frequency space (Grinsted et al., 2004). The continuous wavelet transforms for each signal (W^a, W^b) and the cross-wavelet transform (W^{ab}) are calculated locally at each time (t) and scale (s). The wavelet scale can be converted to frequency using the scale-frequency conversion of the mother wavelet. A smoothing operator (S) is applied in both the time and scale directions to enable comparison of trends in signals a and b. (B) Kinematic traces and cerebrospinal fluid pressure (CSFP) (left) and corresponding wavelet coherence plots (right) for one exemplar E2 test (P1, see Supplementary Figs. S1-S3 for other whiplash exposures). Wavelet coherence plots show regions with significant coherence (yellowish regions inside the black contour lines, determined at alpha = 0.05 compared to a stochastic Gaussian process) and regions in the cone of influence (lighter shaded area below white line) subject to edge effects. The vertical dashed lines indicate the time range of interest (motion onset to maximum head angular displacement). Note that the frequency axis is plotted on a log scale.

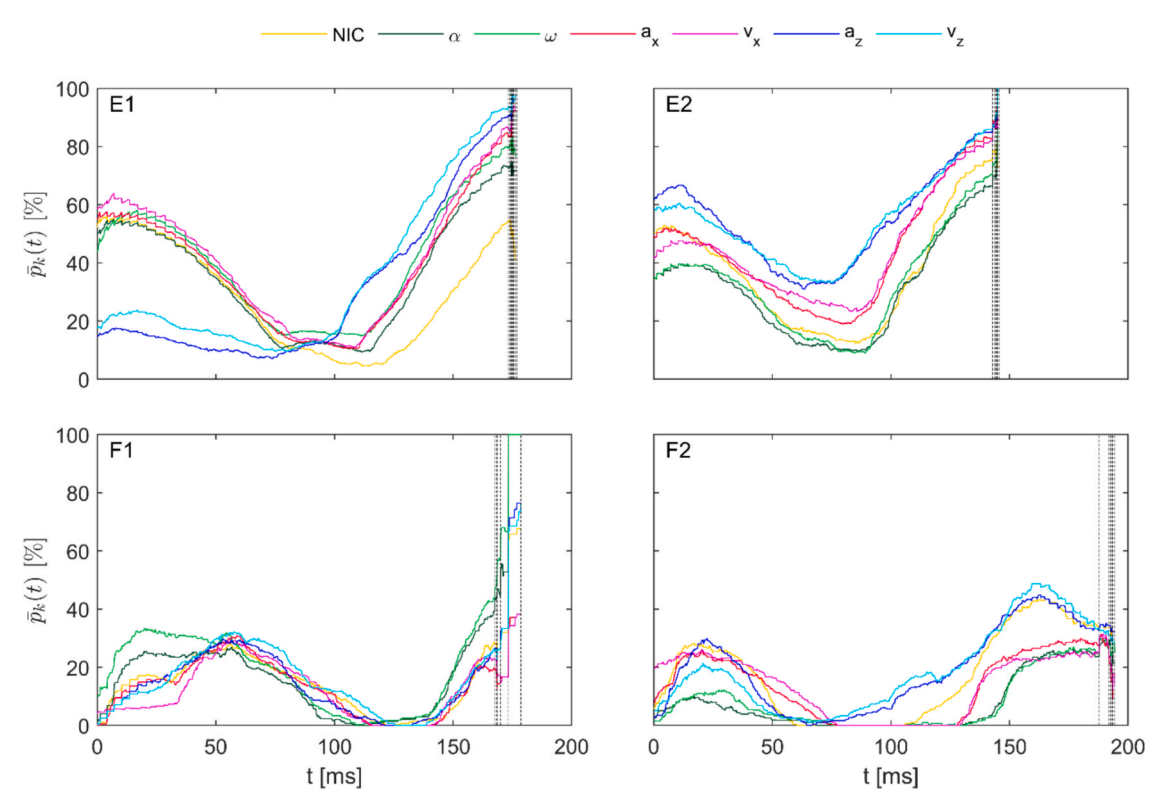


Fig. 4. Mean proportion of significant coherence as a function of time $(\bar{p}_k(t))$ for each kinematic parameter for the E1, E2, F1, and F2 whiplash exposures. Each trace represents a different kinematic parameter. Vertical dashed lines indicate the time at maximum head angular displacement for each test.

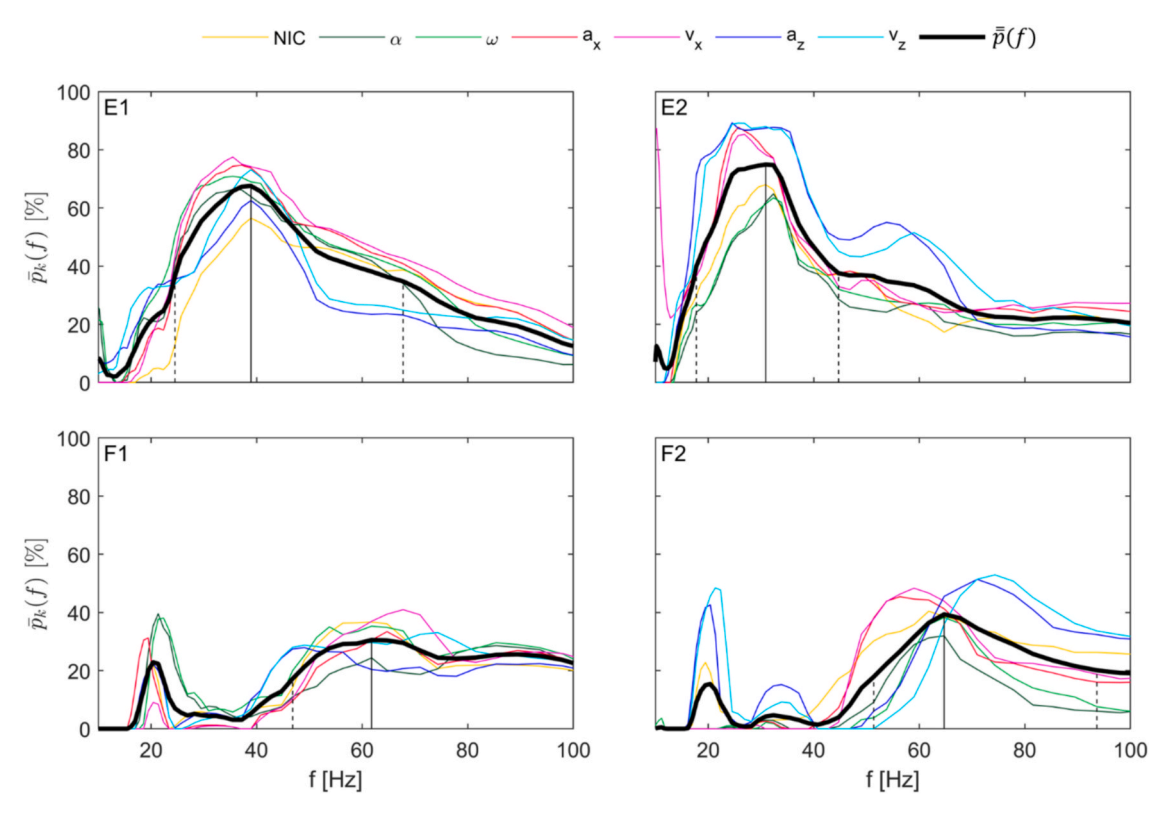


Fig. 5. Mean proportion of significant coherence as a function of frequency $(\bar{p}_k(f))$ for each kinematic parameter for the E1, E2, F1, and F2 whiplash exposures. Each trace represents a different kinematic parameter. The aggregated average across all kinematic parameters $(\bar{p}(f))$, thick solid line) was used to determine the maximal coherence frequency (F, solid vertical line) and the full-width half maximum range (F_{FWHM} , dashed vertical lines).

Table 3 Maximum $\bar{p}(f)$ and corresponding frequency (F) and the full-width half maximum (F_{FWHM}) range for each whiplash exposure.

	$\operatorname{Max} \overline{\overline{p}}(f)$ [%]	F [Hz]	F _{FWHM} Range [Hz]
E1	67.6	38.9	24.5, 67.8
E2	74.9	30.9	17.7, 44.7
F1	30.5	61.8	46.8, >100
F2	39.4	64.7	51.4, 93.6

of this on CSFP transients.

Among the assessed head kinematic parameters, angular and dorsal–ventral head kinematics correlated to CSFP better than the other head kinematics for the E1 whiplash exposures. In contrast, no single head kinematic parameter outperformed the others in the E2, F1, and F2 whiplash exposures. Temporal NIC was a better correlate of CSFP than angular acceleration in F2 but otherwise was either a comparable or a worse correlate of CSFP than other head kinematics measures. NIC was previously derived using a one-dimensional Navier-Stokes equation to model the pressure along the spinal canal (Bostrom et al., 1996) and anterior-posterior kinematics in the global reference frame are conventionally used in the NIC equation without a strong empirical basis. Overall, our findings indicate that the mechanics of CSFP response during whiplash exposures are complex, multidirectional, and may only partially be captured by temporal NIC.

This study has several limitations. Due to the resource-intensity of large-animal studies, only four animals were used, and each animal was necessarily tested repeatedly. However, animals remained medically stable during testing, and head kinematics and CSFP responses were repeatable (Soltan et al., 2025), indicating minimal change in mechanical and physiological response of the neck over the test course. Using the four animals, four different whiplash exposures were simulated with varying number of repeated tests. The smaller sample size of the flexion tests may have affected the statistical findings (or lack thereof). The translation of our findings to humans is limited by the anatomical differences between pigs and humans. Despite some inter-species differences, the pig cervical spine is a reasonable model of the human cervical spine in terms of biomechanical properties and scale (Busscher et al.,

2010; Sheng et al., 2010; Wilke et al., 2011). Given this similar scale, we applied translations and rotations to the head that were based on human subject tests. Importantly, the extension exposures in this study did not model the interaction with, or protective effect of, a head restraint, and may represent a more extreme loading scenario than some rear-end collisions with a head restraint. In real-world whiplash exposures, the collision forces are transferred to the neck and head via the torso, whereas in the whiplash exposures used here, the forces were applied to head while maintaining a stationary torso. This difference in the inertial loading direction and the use of a biteplate could affect the sequence and dynamics of the intervertebral motion and consequently the origin and propagation of the CSFP transients. The effect of this difference, if any, requires further investigation. All head kinematics in this study were transformed to a generic pig AOJ location defined previously (Soltan et al., 2023). Though this AOJ location is based on domestic pigs of comparable size and sex as in this study, absence of subject-specific AOJ transformations could have introduced errors into the calculated AOJ kinematics. The intrathecal insertion of pressure transducers inevitably involved some CSF loss (~5 mL from pilot work). However, this loss was likely restored during the span from sealing the catheter-dura interface to the first whiplash exposure (4.6 \pm 0.7 hrs; assuming a CSF formation rate comparable to goats, 0.1 mL/min (Seckl and Lightman, 1991)). Finally, cervical CSFP was measured in the intrathecal space at the midvertebral level. Exact placement of the pressure transducers at the nerve roots or dorsal root ganglia was not possible without laminectomies in the cervical spine which would disrupt head/neck kinematics.

In conclusion, using an *in vivo* pig model, we characterized the time–frequency relationship between head kinematics and cervical CSFP transients in extension and flexion whiplash exposures. Head kinematics were better correlated with CSFP in extension exposures than flexion exposures. These correlations peaked in the first and last 50 ms of exposures, and between 30–65 Hz for both extension and flexion exposures. As an existing whiplash injury criterion, NIC was not universally a better correlate of CSFP response than other head kinematic measures. These findings suggest that whiplash injury criteria related to the potential hydrodynamic loading of neural tissue may need to account for the complex intervertebral dynamics during exposures. A deeper mechanistic understanding of the CSFP-based whiplash injury

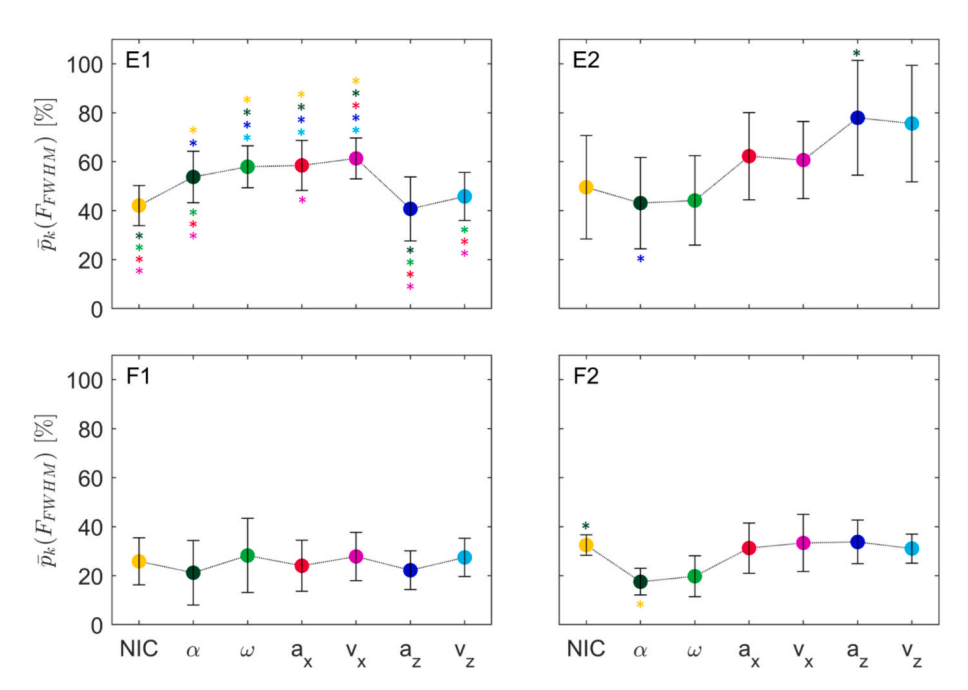


Fig. 6. Mean and standard deviation of $p_{ki}(F_{FWHM})$ for each CSFP-kinematic parameter pair. Statistically significant differences (p-value < 0.05) indicated by color coded * and placed above the data point if the mean in question is larger than the comparator, and below the data point if the mean in question is smaller than the comparator. Pairwise comparisons not made for F1 (overall F-statistic was not significant). Refer to Supplementary Tables S1-S4 for tabulated results.

mechanism could help improve whiplash injury criteria.

CRediT authorship contribution statement

Nikoo Soltan: Writing – review & editing, Writing – original draft, Visualization, Validation, Project administration, Methodology, Investigation, Formal analysis, Data curation. Mats Y. Svensson: Writing – review & editing, Methodology, Funding acquisition, Conceptualization. Claire F. Jones: Writing – review & editing, Methodology. Peter A. Cripton: Writing – review & editing, Validation, Supervision, Resources, Project administration, Methodology, Investigation, Funding acquisition, Formal analysis, Conceptualization. Gunter P. Siegmund: Writing – review & editing, Validation, Supervision, Resources, Project administration, Methodology, Investigation, Funding acquisition, Formal analysis, Conceptualization.

Declaration of competing interest

Author GPS is a director and minority shareholder in a forensic engineering consulting company. The remaining authors declare that they have no known competing financial interests or personal relationships that could have appeared to influence the work reported in this paper.

Acknowledgments

The authors are grateful for the technical support of the staff and veterinary team at the University of British Columbia Center for Comparative Medicine, and Jeff Nickel and Mircea Oala-Florescu at MEA Forensic Engineers & Scientists. We also acknowledge the staff at the South Australian Health and Medical Research Institute Preclinical, Imaging and Research Laboratories for their assistance during pilot work. Project funding was provided by the Insurance Institute for Highway Safety, the Natural Sciences and Engineering Research Council of Canada, and Folksams Forskningsstiftelse, Sweden.

Appendix A. Supplementary data

Supplementary data to this article can be found online at https://doi.org/10.1016/j.jbiomech.2025.112994.

References

- Aldman, B., 1986. An analytical approach to the impact biomechanics of head and neck injury. 30th Annu. Proc. Am. Assoc. Automot. Med. 31, 2075–2093.
- Aprill, C., Dwyer, A., Bogdukl, N., 1990. Cervical zygapophyseal joint paint patterns II: A clinical evaluation. Spine (Phila Pa 1976) 15, 458–461.
- Bertholon, N., Robin, S., Le-Cos, J., Potier, P., Lassau, J., Skalli, W., 2000. Human head and cervical spine behaviour during low-speed rear-end impacts: PMHS sled tests with a rigid seat. Proc IRCOBI Conf 3.
- Bostrom, O., Svensson, M., Aldman, B., Hansson, H., Haland, Y., Lovsun, P., Seeman, T., Suneson, A., Saljo, A., Ortengren, T., 1996. A new neck injury criterion candidatebased on injury findings in the cervical spinal ganglia after experimental neck extension trauma. Proc. IRCOBI Conf. 123–136.
- Bourdet, N., Fischer, R., Willinger, R., 2005. Human neck characterization under thoracic vibration Inter-individual and gender influence. Proc. IRCOBI Conf. 257–267.
- Busscher, I., Ploegmakers, J.J.W., Verkerke, G.J., Veldhuizen, A.G., 2010. Comparative anatomical dimensions of the complete human and porcine spine. Eur. Spine J. 19, 1104–1114. https://doi.org/10.1007/s00586-010-1326-9.
- Chien, A., Eliav, E., Sterling, M., 2010. The development of sensory hypoesthesia after whiplash injury. Clin. J. Pain 26, 722–728. https://doi.org/10.1097/ AJP.0b013e3181f096ac.
- Chien, A., Eliav, E., Sterling, M., 2009. Hypoaesthesia occurs with sensory hypersensitivity in chronic whiplash - further evidence of a neuropathic condition. Man. Ther. 14, 138–146. https://doi.org/10.1016/j.math.2007.12.004.
- Chien, A., Eliav, E., Sterling, M., 2008. Whiplash (Grade II) and cervical radiculopathy share a similar sensory presentation: an investigation using quantitative sensory testing. Clin. J. Pain 24, 595–603. https://doi.org/10.1097/AJP.0b013e31816ed4fc.
- Curatolo, M., Bogduk, N., Ivancic, P.C., McLean, S.A., Siegmund, G.P., Winkelstein, B.A., 2011. The role of tissue damage in whiplash-associated disorders. Spine (Phila. Pa. 1976) 36, S309–S315. https://doi.org/10.1097/BRS.0b013e318238842a.

- Deng, B., Melvin, J.W., Rouhana, S.W., 1998. Head-Neck Kinematics in Dynamic Forward Flexion. SAE Tech Pap.
- Elliott, J.M., Noteboom, J.T., Flynn, T.W., Sterllng, M., 2009. Characterization of acute and chronic whiplash-associated disorders. J. Orthop. Sports Phys. Ther. 39, 312–323. https://doi.org/10.2519/jospt.2009.2826.
- Fundaun, J., Kolski, M., Baskozos, G., Dilley, A., Sterling, M., Schmid, A.B., 2022. Nerve pathology and neuropathic pain after whiplash injury: a systematic review and meta-analysis. Pain 163, E789–E811. https://doi.org/10.1097/j.pain.000000000002509.
- Grinsted, A., Moore, J.C., Jevrejeva, S., 2004. Application of the cross wavelet transform and wavelet coherence to geophysical time series. Nonlinear Process. Geophys. 11, 561–566. https://doi.org/10.5194/npg-11-515-2004.
- Hoggarth, M.A., Elliott, J.M., Smith, Z.A., Paliwal, M., Kwasny, M.J., Wasielewski, M., Weber, K.A., Parrish, T.B., 2020. Macromolecular changes in spinal cord white matter characterize whiplash outcome at 1-year post motor vehicle collision. Sci. Rep. 10, 1–10. https://doi.org/10.1038/s41598-020-79190-5.
- Holmes, A., Han, H.Z., Dang, G.T., Chen, Z.Q., Wang, Z.G., Fang, J., 1996. Changes in cervical canal spinal volume during in vitro flexion-extension. Spine (Phila. Pa. 1976) 21, 1313–1319.
- Kang, Y.-S., Stammen, J., Moorhouse, K., Bolte IV, J., 2018. Head and neck responses of post mortem human subjects in frontal, oblique, side and twist scenarios. Proc. IRCOBI Conf. 114–124.
- Maraun, D., Kurths, J., 2004. Cross wavelet analysis: significance testing and pitfalls. Nonlinear Process. Geophys. 11, 505–514. https://doi.org/10.5194/npg-11-363-2004
- Moroney, S.P., Schultz, A.B., Miller, J.A.A., Andersson, G.B.J., 1988. Load-displacement properties of lower cervical spine motion segments. J. Biomech. 21, 769–779. https://doi.org/10.1016/0021-9290(88)90285-0.
- Örtengren, T., Hansson, H.A., Lövsund, P., Svensson, M.Y., Suneson, A., Saljö, A., 1996. Membrane leakage in spinal ganglion nerve cells induced by experimental whiplash extension motion: a study in pigs. J. Neurotrauma 13, 171–180. https://doi.org/10.1089/neu.1996.13.171.
- Panjabi, M.M., Crisco, J.J., Vasavada, A.N., Oda, T., Cholewicki, J., Nibu, K., Shin, E., 2001. Mechanical properties of the human cervical spine as shown by three-dimensional load-displacement curves. Spine (Phila. Pa. 1976) 26, 2692–2700. https://doi.org/10.2106/00004623-197658050-00011.
- Panjabi, M.M., Maak, T.G., Ivancic, P.C., Ito, S., 2006. Dynamic intervertebral foramen narrowing during simulated rear impact. Spine (Phila. Pa. 1976) 31, 128–134. https://doi.org/10.1097/01.brs.0000201243.81745.ba.
- Ridehalgh, C., Fundaun, J., Bremner, S., Cercignani, M., Koushesh, S., Young, R., Novak, A., Greening, J., Schmid, A.B., Dilley, A., 2025. Evidence for peripheral neuroinflammation after acute whiplash. Pain 00, 1–15. https://doi.org/10.1097/j. pain.0000000000003560.
- SAE, 2003. SAE recommended practice: Instrumentation for impact tests (SAE J211-1 Dec 03). Soc. Automot. Eng. Handb.
- Seckl, J.R., Lightman, S.L., 1991. Intracerebroventricular vasopressin reduces CSF absorption rate in the conscious goat. Exp. Brain Res. 84, 173–176. https://doi.org/ 10.1007/BF00231772.
- Shea, M., Edwards, W.T., White, A.A., Hayes, W.C., 1991. Variations of stiffness and strength along the human cervical spine. J. Biomech. 24. https://doi.org/10.1016/ 0021-9290(91)90354-P.
- Sheng, S.R., Wang, X.Y., Xu, H.Z., Zhu, G.Q., Zhou, Y.F., 2010. Anatomy of large animal spines and its comparison to the human spine: a systematic review. Eur. Spine J. 19, 46–56. https://doi.org/10.1007/s00586-009-1192-5.
- Siegmund, G.P., King, D.J., Lawrence, J.M., Wheeler, J.B., Brault, J.R., Smith, T.A., 1997. Head/neck Kinematic Response of Human Subjects in Low-Speed Rear-End Collisions. Soc. Automot. Eng.
- Siegmund, G.P., Winkelstein, B.A., Ivancic, P.C., Svensson, M.Y., Vasavada, A., 2009. The anatomy and biomechanics of acute and chronic whiplash injury. Traffic Inj. Prev. 10, 101–112. https://doi.org/10.1080/15389580802593269.
- Soltan, N., Siegmund, G.P., Cripton, P.A., Jones, C.F., 2023. Geometric and inertial properties of the pig head and brain in an anatomical coordinate system. Ann. Biomed. Eng. 51, 2544–2553. https://doi.org/10.1007/s10439-023-03294-y.
- Soltan, N., Svensson, M.Y., Jones, C.F., Cripton, P.A., Siegmund, G.P., 2025. In vivo pressure responses of the cervical cerebrospinal fluid in a porcine model of extension and flexion whiplash exposures. Ann. Biomed. Eng. 1–15. https://doi.org/10.1007/ s10439-025-03695-1.
- Sterling, M., Jull, G., Vicenzino, B., Kenardy, J., 2004. Characterization of acute whiplash-associated disorders. Spine (Phila. Pa. 1976) 29, 182–188.
- Svensson, M.Y., Aldman, B., Hansson, H., Lövsund, P., Seeman, T., Suneson, A., Örtengren, T., 1993. Pressure effects in the spinal canal during whiplash extension motion: a possible cause of injury to the cervical spinal ganglia. Proc. IRCOBI Conf. 189–200.
- Svensson, M.Y., Boström, O., Davidsson, J., Hansson, H.A., Håland, Y., Lövsund, P., Suneson, A., Säljö, A., 2000. Neck injuries in car collisions a review covering a possible injury mechanism and the development of a new rear-impact dummy. Accid. Anal. Prev. 32, 167–175. https://doi.org/10.1016/S0001-4575(99)00080-9.
- Van Oosterwijck, J., Nijs, J., Meeus, M., Paul, L., 2013. Evidence for central sensitization in chronic whiplash: a systematic literature review. Eur. J. Pain 17, 299–312. https://doi.org/10.1002/j.1532-2149.2012.00193.x.
- Wilke, H.J., Geppert, J., Kienle, A., 2011. Biomechanical in vitro evaluation of the complete porcine spine in comparison with data of the human spine. Eur. Spine J. 20, 1859–1868. https://doi.org/10.1007/s00586-011-1822-6.